ISOTROPY AND HOMOGENEITY OF THE TAYLOR-GREEN-VORTEX

Markus Klein
Department of Aerospace Engineering, University of the Bundeswehr Munich,
Werner-Heisenberg-Weg 39, 85577 Neubiberg, Germany, markus.klein@unibw.de

Artur Tyliszczak
Department of Thermal Machinery, Czestochowa University of Technology,
Al. Armii Krajowej 21, 42-201 Czestochowa, Poland, artur.tyliszczak@pcz.pl

Josef Hasslberger
Department of Aerospace Engineering, University of the Bundeswehr Munich,
Werner-Heisenberg-Weg 39, 85577 Neubiberg, Germany, josef.hasslberger@unibw.de

Massimo Germano
Department of Civil and Environmental Engineering, Duke University,
121 Hudson Hall, Durham, NC 27708, USA, mg234@duke.edu

ABSTRACT

The Taylor–Green vortex (TGV) is commonly used as a benchmark for laminar turbulent transition and is often assumed to approach homogeneous isotropic turbulence (HIT) at late stages. Using direct numerical simulations of the standard and an isotropic TGV, we assess this assumption based on Reynolds stress anisotropy, integral length scales, and homogeneity indices derived from mixed averaging procedures. The results show that the standard TGV remains anisotropic, while the isotropic variant, although initially isotropic by construction, does not reproduce key characteristics of HIT. In both configurations, persistent spatial inhomogeneities are observed, indicating that the flow does not fully approach a homogeneous isotropic state.

INTRODUCTION

The Taylor–Green vortex (TGV) (Taylor & Green, 1937) represents a simple yet well-defined flow configuration that exhibits rich physical phenomena, including laminar-to-turbulent transition, posing a significant challenge for large-eddy simulation (LES) models. Owing to its straightforward, fully periodic setup, it has long served as a canonical benchmark for analyzing turbulence dynamics (Orszag, 1974; Brachet *et al.*, 1983) and for the development and assessment of LES methodologies (Domaradzki *et al.*, 1993; Hickel *et al.*, 2006; Reissmann *et al.*, 2021; Engelmann *et al.*, 2023; Hasslberger *et al.*, 2025; Caban *et al.*, 2026). The temporal evolution of the TGV is characterized by a laminar initial state, followed by nonlinear instability, energy cascade, and eventual decay due to viscous dissipation. During the turbulent stage, the flow is often assumed to approximate homogeneous isotropic turbulence (HIT). While early studies showed that the flow retains anisotropic features at large scales, small-scale isotropy may be approached at sufficiently high Reynolds numbers (Brachet *et al.*, 1983; Hickel *et al.*, 2006). However, isotropy and homogeneity impose stringent requirements, namely directional and spatial invariance of statistical quantities. In flows such as the TGV, symmetry-preserving initial conditions and finite periodic domains constrain the dynamics and may prevent complete homogenization and isotropization (Bardos *et al.*, 2013). Recent results indicate persistent anisotropy in plane-averaged statistics, suggesting a lasting imprint of the initial condition (Engelmann *et al.*, 2023). Despite its widespread use, a systematic assessment of both isotropy and homogeneity, particularly for different initial conditions, remains limited. From a theoretical perspective, small-scale isotropization is expected as a consequence of the turbulent energy cascade (Kolmogorov, 1941; Frisch, 1995), whereas large-scale motions may retain memory of the flow configuration. Nevertheless, the TGV is frequently interpreted as approaching a homogeneous or homogeneous-isotropic state at late times (Kulikov & Son, 2018; Nathen *et al.*, 2018). Assessing the validity of this assumption is essential for its use as a benchmark in turbulence modeling. In this work, we analyze the isotropy and homogeneity of both the standard TGV and an isotropic variant (Ono *et al.*, 2024). A suite of statistical measures is employed, including Reynolds stress anisotropy, integral length scales, and homogeneity indices based on mixed averaging procedures. The focus is on the late decay stage, where the flow is commonly assumed to resemble HIT. The present contribution summarizes key findings from a more extensive study reported by Klein *et al.* (2026).

PROBLEM DESCRIPTION

The TGV flow, with its well known and simple case-design, is a prominent benchmark for the study of free laminar-

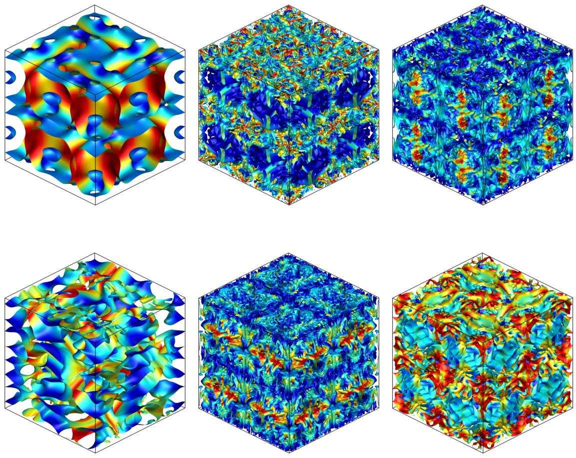

Figure 1. Q-criterion iso-surfaces of the *standard* TGV (top) and the *isotropic* TGV (bottom) at a value of zero colored using $|U|/|U_{max}|$ at dimensionless times of $t/t_0 = 2.0$, $t/t_0 = 10.0$ and $t/t_0 = 25.0$ from left to right.

turbulent transition (Brachet *et al.*, 1983). The domain features a length of 2π in each dimension. The initial velocity field is given by the following expressions:

$$\begin{aligned} u(x,y,z) &= U_0 \cos(x) \sin(y) \sin(z) \\ v(x,y,z) &= -U_0 \sin(x) \cos(y) \sin(z) \\ w(x,y,z) &= 0 \end{aligned} \tag{1}$$

with the reference velocity $U_0 = 1$ m/s, timescale $t_0 = 1$ s and length $l_0 = 1$ m. The Reynolds number of $Re = \rho U_0 l_0/\mu = 1600$ at the initialization is achieved by setting the density to $\rho = 1 kg/m^3$ and dynamic viscosity to $\mu = 0.625 \cdot 10^{-3} Pa\, s$. Using a modified initial condition Ono *et al.* (2024) introduced the *isotropic* TGV. Its initialization reads

$$\begin{aligned} u(x,y,z) &= U_0/\sqrt{6}\left(-\cos(x)\sin(y) + \cos(x)\sin(z)\right) \\ v(x,y,z) &= U_0/\sqrt{6}\left(-\cos(y)\sin(z) + \cos(y)\sin(x)\right) \\ w(x,y,z) &= U_0/\sqrt{6}\left(-\cos(z)\sin(x) + \cos(z)\sin(y)\right) \end{aligned} \tag{2}$$

and the reference time is chosen to be twice that of the standard TGV for comparison.

THEORETICAL BACKGROUND

The TGV will be analyzed using quantities that characterize the effects of turbulence, such as Reynolds stresses $R_{ij} = \langle u_i u_j \rangle - \langle u_i \rangle \langle u_j \rangle$, turbulent kinetic energy $k = R_{ii}/2$ and coherent structure function F_{CS} (Kobayashi, 2005). The angled brackets denote a suitable averaging operation. Averaging is either performed globally in space or along $x-y$ planes and lines at a fixed instant in time. In the latter case, the resulting profiles will be plotted as a function of the plane-normal direction z. The coherent structure function is defined as $F_{CS} = Q/E$ which is the ratio of the second invariant of the velocity gradient tensor Q and its respective squared magnitude E:

$$Q = -\frac{1}{2}\frac{\partial u_j}{\partial x_i}\frac{\partial u_i}{\partial x_j} \qquad E = \frac{1}{2}\frac{\partial u_j}{\partial x_i}\frac{\partial u_j}{\partial x_i} \tag{3}$$

The coherent structure function is an instructive quantity, as it captures the relationship between dissipation and enstrophy, two fundamental measures used to characterize the structure of turbulent flows. Being a strictly bounded quantity $(-1 < F_{CS} < +1)$, it exhibits mathematical elegance, and the iso-contour $F_{CS} = 0$ identifies the state of dissipation-

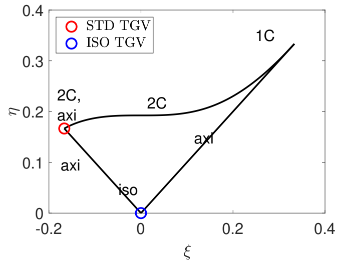

Figure 2. Anisotropy of Reynolds stresses in the Lumley triangle, shown for the standard and isotropic TGV flow at $t/t_0 = 0$. The following abbreviations are used: 1C: one-component, 2C: two-component, axi: axisymmetric, iso: isotropic.

enstrophy equilibrium. Moreover, F_{CS} can be interpreted as a suitably normalized form of the Q-criterion, which is commonly employed in the literature to detect enstrophy-dominated regions in turbulent flows.

The anisotropy in a turbulent flow can be conveniently characterized with the help of the Lumley triangle (Lumley, 1979). Its boundaries are given as a function of the second and third invariant of the anisotropy tensor $a_{ij} = R_{ij}/R_{kk} - \delta_{ij}/3$ and by introducing the variables η, ξ

$$\mathrm{II}(a) = \left(\mathrm{trace}(a)^2 - \mathrm{trace}\left(a^2\right)\right)/2, \;\; \mathrm{III}(a) = (\det(a)) \tag{4}$$

$$\eta = (-\mathrm{II}(a)/3)^{1/2}, \quad \xi = (-\mathrm{III}(a)/2)^{1/3}. \tag{5}$$

Any physically realizable state of the anisotropy tensor a_{ij} lies within the triangle shown exemplarily in Fig. 2 for the standard and isotropic TGV at initialization, i.e. $t/t_0 = 0$. The left and right borders of the triangle represent an axisymmetric contraction and expansion, respectively, while the upper border denotes the two-component state. Finally, the isotropic state corresponds to the lower corner $(\xi, \eta) = (0,0)$.

The homogeneity of the TGV will be analyzed by a homogeneity measure introduced by Germano and co-workers (Errante *et al.*, 2024). It is based on considering a mixed averaging procedure, where $\langle \cdot \rangle_\alpha$ denotes averaging in (homogeneous) direction x_α, $\langle \cdot \rangle_{\alpha\beta}$ denotes averaging in both (homogeneous) directions x_α, x_β and $\langle \cdot \rangle_{\alpha\beta\gamma}$ for averaging in volume. In the general case, time averaging can be included as well, but this does not apply for the TGV, because of its unsteady nature. The choice of the averaging procedure gives rise to a generalized central moment (Germano, 1992), signifying the Reynolds stresses determined from averaging in the given direction(s) (when applied to the velocity components):

$$\tau_\alpha(u_i, u_j) = \langle u_i u_j \rangle_\alpha - \langle u_i \rangle_\alpha \langle u_j \rangle_\alpha, \tag{6}$$

$$\tau_{\alpha\beta}(u_i, u_j) = \langle u_i u_j \rangle_{\alpha\beta} - \langle u_i \rangle_{\alpha\beta} \langle u_j \rangle_{\alpha\beta}, \;\; \ldots \tag{7}$$

Averaging τ_α in β direction and making use of $\langle\langle \cdot \rangle_\alpha\rangle_\beta = \langle\langle \cdot \rangle_\beta\rangle_\alpha = \langle \cdot \rangle_{\alpha\beta}$ results in

$$\langle \tau_\alpha(u_i, u_j)\rangle_\beta = \langle u_i u_j \rangle_{\alpha\beta} - \langle \langle u_i \rangle_\alpha \langle u_j \rangle_\alpha \rangle_\beta, \tag{8}$$

Inserting Eq. 8 into Eq. 7 and using $\tau_\beta(\langle u_i \rangle_\alpha, \langle u_j \rangle_\alpha) = \langle\langle u_i \rangle_\alpha \langle u_j \rangle_\alpha\rangle_\beta - \langle\langle u_i \rangle_\alpha\rangle_\beta \langle\langle u_j \rangle_\alpha\rangle_\beta$ gives finally rise to

$$\begin{aligned} \tau_{\beta\alpha}(u_i, u_j) &= \langle \tau_\alpha(u_i, u_j)\rangle_\beta + \tau_\beta(\langle u_i \rangle_\alpha, \langle u_j \rangle_\alpha) \\ &= \langle \tau_\beta(u_i, u_j)\rangle_\alpha + \tau_\alpha(\langle u_i \rangle_\beta, \langle u_j \rangle_\beta) = \tau_{\alpha\beta}(u_i, u_j) \end{aligned} \tag{9}$$

for a 2D partition, and

$$\begin{aligned} \tau_{\gamma\beta\alpha}(u_i, u_j) &= \langle \tau_\alpha(u_i, u_j)\rangle_{\beta\gamma} + \tau_{\beta\gamma}(\langle u_i \rangle_\alpha, \langle u_j \rangle_\alpha) = \\ &= \langle \tau_{\alpha\beta}(u_i, u_j)\rangle_\gamma + \tau_\gamma(\langle u_i \rangle_{\alpha\beta}, \langle u_j \rangle_{\alpha\beta}) = \cdots \end{aligned} \tag{10}$$

for a 3D partition of the statistical measure. Based on this, we define the following measures of homogeneity in 2D partitions

$$M_{\alpha(\beta)}(u_i,u_j) = \frac{\langle \tau_\alpha(u_i,u_j)\rangle_\beta}{\tau_{\beta\alpha}(u_i,u_j)} = 1 - \frac{\tau_\beta(\langle u_i\rangle_\alpha, \langle u_j\rangle_\alpha)}{\tau_{\beta\alpha}(u_i,u_j)} \quad (11)$$

and the following in 3D partitions

$$M_{\alpha(\beta\gamma)}(u_i,u_j) = \frac{\langle \tau_\alpha(u_i,u_j)\rangle_{\beta\gamma}}{\tau_{\gamma\beta\alpha}(u_i,u_j)} = 1 - \frac{\tau_{\beta\gamma}(\langle u_i\rangle_\alpha, \langle u_j\rangle_\alpha)}{\tau_{\gamma\beta\alpha}(u_i,u_j)}. \quad (12)$$

These indices allow for quantification of the relative contribution by averaging in different directions to the evaluation of the statistics. For example an index of $M_{\alpha(\beta\gamma)} \approx 1$ indicates that Reynolds stresses are equally well captured for $\tau_{\alpha\beta\gamma}$ and τ_α statistics. From a probabilistic point of view this implies that there is a sufficient number of statistically independent samples in x_α direction. If the diagonal components of the Reynolds stresses are considered, i.e., $i=j$, we write in the following more briefly $M_{\alpha\beta(\gamma)}(u_i)$ instead of $M_{\alpha\beta(\gamma)}(u_i,u_i)$. For an isotropic flow, the quantity $M_{\alpha(\beta\gamma)}(u_i)$ should, in a statistical sense, be the same under rotation of the coordinate system, i.e. $M_{x(yz)}(u) = M_{y(xz)}(v) = M_{z(xy)}(w)$ and $M_{y(xz)}(u) = M_{z(xy)}(u) = M_{x(yz)}(v) = M_{z(xy)}(v) = M_{x(yz)}(w) = M_{y(xz)}(w)$.

In turbulent flows, the number of statistically independent spatial samples is inversely proportional to the integral length scale, which is obtained by integrating the appropriate normalized two-point correlation function

$$\chi_{\phi,\psi,i}(\vec{x},r) = \langle \phi(\vec{x}), \psi(\vec{x}+\vec{e}_i r)\rangle / \langle \phi(\vec{x}), \psi(\vec{x})\rangle \quad (13)$$

from $r=0\ldots r_+$, where r_+ denotes the first root such that $\chi_{\phi,\psi,i}(\vec{x},r_+) = 0$ (i.e., the positive lobe convention is applied). For the TGV, the averaging operator $\langle\cdot\rangle$ is taken over all three spatial directions, allowing the dependence on $\vec{x}$ to be omitted. The integral length scale is defined as

$$L_{\phi\psi,i} = \int_0^{r_+} \chi_{\phi,\psi,i}(r)dr \quad (14)$$

In the case of the velocity field, the longitudinal integral length scales are denoted compactly as $L_{ii,i}$ (in place of $L_{u_iu_i,i}$) and, analogously, the transverse length scales as $L_{ii,j}$ for $i \neq j$. Knowing that for homogeneous, isotropic turbulence, the longitudinal and transverse length scales are related by $L_{ii,i} = 2L_{ii,j\neq i}$ (Pope, 2000), we will examine whether or to what extent the above relation holds for the TGV evolution.

NUMERICAL SETUP

Simulations are performed using the high-order finite-difference code SAILOR, which employs a projection method for velocity–pressure coupling. Time integration is based on a 2^{nd} order Adams–Bashforth / Adams–Moulton predictor–corrector scheme, and spatial discretization uses a 10^{th}-order compact finite-difference method on a half-staggered grid (Tyliszczak, 2014, 2016). The computations are carried out on a uniform mesh with $N=256$ nodes in each spatial direction. The time step is set to $\Delta t = 10^{-3}$s ($CFL \approx 0.04$), and simulations are run up to $t = 100t_0$. The grid satisfies $\eta_K/h = 0.49, 0.67$ for the *standard* and *isotropic* TGV, respectively, ensuring resolution of the smallest scales (Pope, 2000). The results show very good agreement with available reference DNS (Brachet *et al.*, 1983; Hillewaert, K., 2011).

RESULTS

The global statistics in Fig. 3 indicate that both configurations exhibit similar overall TKE decay behavior when scaled with the characteristic time t_0. However, clear differences arise in the dissipation rate and associated length scales. The

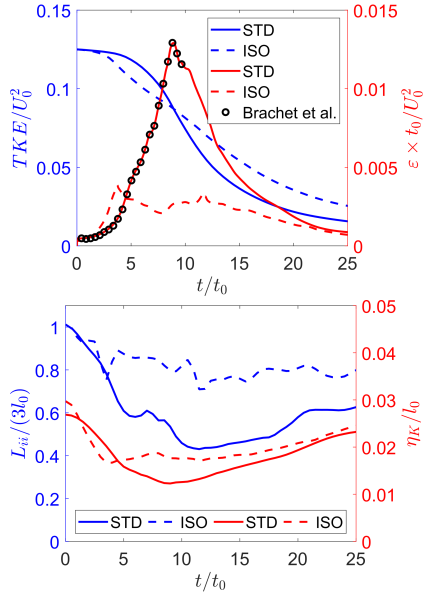

Figure 3. Top: Turbulent kinetic energy and its dissipation. Bottom: Turbulent integral length scales and Kolmogorov scale. All results are shown for the *standard* (STD) and *isotropic* (ISO) TGV. The time scale t_0 for the *isotropic* TGV is twice that of the *standard* TGV.

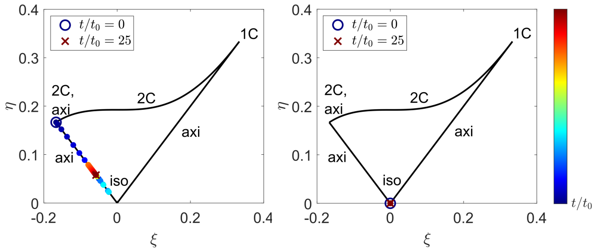

Figure 4. Turbulence state based on Reynolds stresses plotted in the Lumley triangle over time. Left: *standard* TGV. Right: *isotropic* TGV. The time scale t_0 for the *isotropic* TGV is twice that of the *standard* TGV.

isotropic TGV shows a lower peak dissipation and correspondingly larger energy-containing structures, consistent with the increased integral length scales observed in Fig. 7.

The anisotropy evolution shown in Fig. 4 demonstrates that the *standard* TGV does not reach a fully isotropic state, even at late times. While the flow approaches the isotropic point during the peak dissipation phase, it subsequently departs again and remains anisotropic during decay. Subsequently, the flow loses energy rapidly and the isotropy state remains nearly unaffected even up to $t/t_0 = 100$ (not shown in the figure), where it attains the values $(\xi,\eta) = (-0.073, 0.073)$. In contrast, the *isotropic* TGV remains isotropic by construction when assessed using global Reynolds stress statistics. However, this apparent isotropy does not imply that the flow exhibits all characteristics of homogeneous isotropic turbulence.

The Reynolds stresses (note the clear departure from isotropy for the *standard* TGV) and homogeneity indices in Figs. 5 and 6 provide further insight into the spatial structure of the flow. For the *standard* TGV, these indices exhibit clear directional dependence, indicating unequal statistical convergence. This behavior is closely related to the

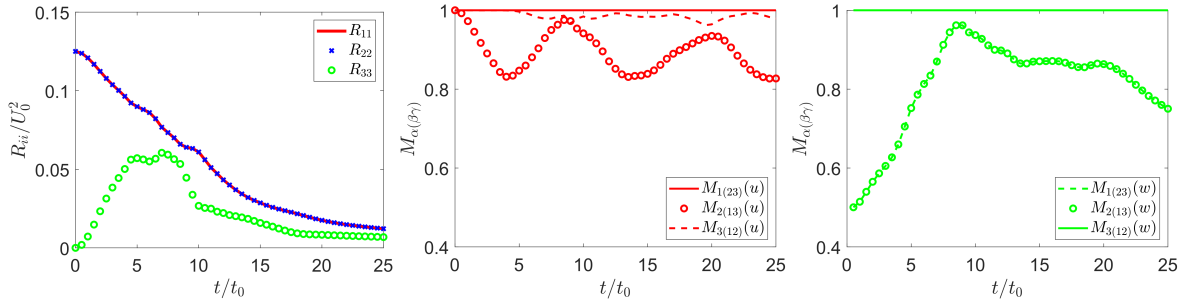

Figure 5. Results for the *standard* TGV. Left: Reynolds stress components $R_{ii}, i = 1,2,3$; Middle and Right: Homogeneity indicies $M_{\alpha(\beta\gamma)}(u_i), i = 1,3$ (u_2 component qualitatively similar to u_1).

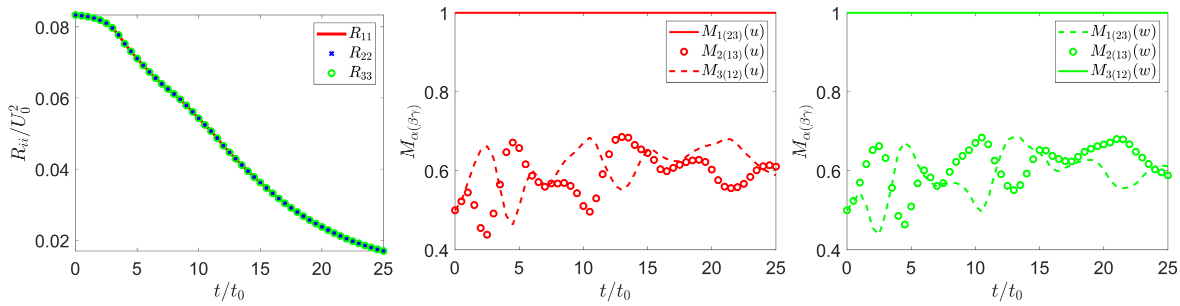

Figure 6. Results for the *isotropic* TGV. Left: Reynolds stress components $R_{ii}, i = 1,2,3$; Middle and Right:: Homogeneity indicies $M_{\alpha(\beta\gamma)}(u_i), i = 1,3$ (u_2 component qualitatively similar to u_1).

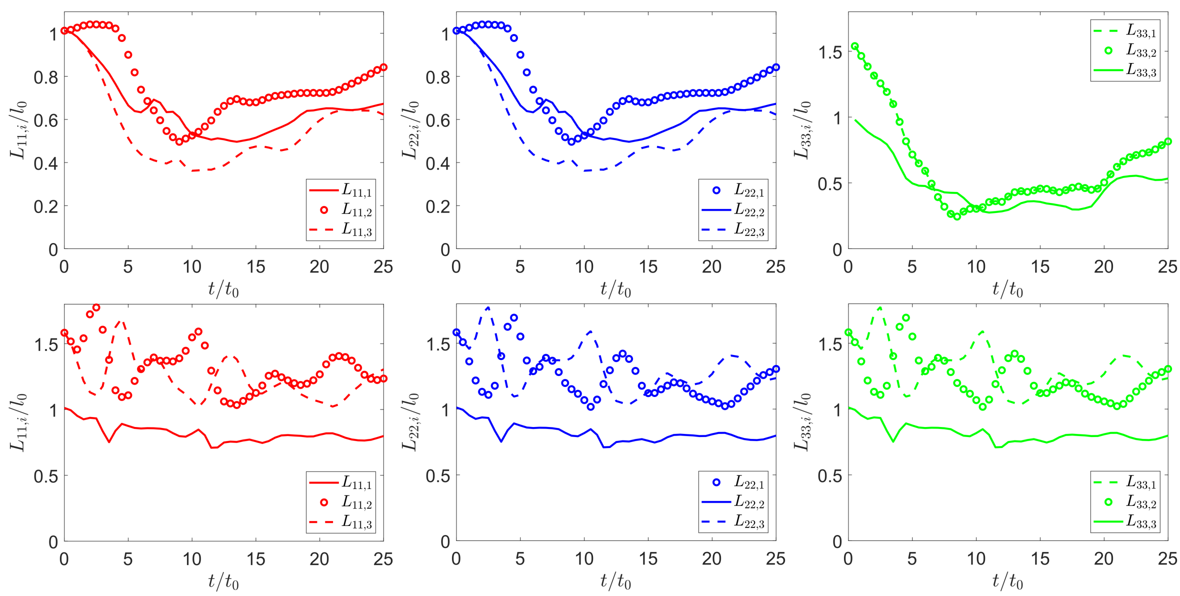

Figure 7. Longitudinal $L_{ii,i}$ and transverse lengthscales $L_{ii,j\neq i}$ for $i = 1,2,3$ for the *standard* (top) and *isotropic* TGV (bottom).

anisotropy of the integral length scales, as larger length scales correspond to a reduced number of statistically independent samples. While the *isotropic* TGV satisfies symmetry constraints of isotropy in these indices, significant deviations from homogeneous isotropic turbulence remain, particularly in the relation between longitudinal and transverse length scales (see Fig. 7).

A more direct indication of inhomogeneity is provided by the plane-averaged statistics in Fig. 8. Both configurations exhibit persistent spatial variations in the z direction, with pronounced peaks in the coherent structure function and turbulent kinetic energy at $z/l_0 = \pi/2, 3\pi/2$. These features remain fixed in space throughout the simulation and are therefore not associated with transient turbulent fluctuations, but rather reflect the underlying symmetry of the initial conditions.

This behavior is further supported by the plane-averaged anisotropy shown in Fig. 9, where the distribution of states in the Lumley triangle varies significantly with z. Even in the *isotropic* TGV, local anisotropy is present despite global isotropy. Although results are shown up to $t/t_0 = 25$, the qualitative behavior remains unchanged when extending the simulation to $t/t_0 = 100$. In particular, the homogeneity indices remain nearly constant, as does the globally averaged anisotropy. Moreover, negative peaks of F_{CS} persist for both TGVs at $t/t_0 = 100$.

Overall, the results indicate that neither configuration ap-

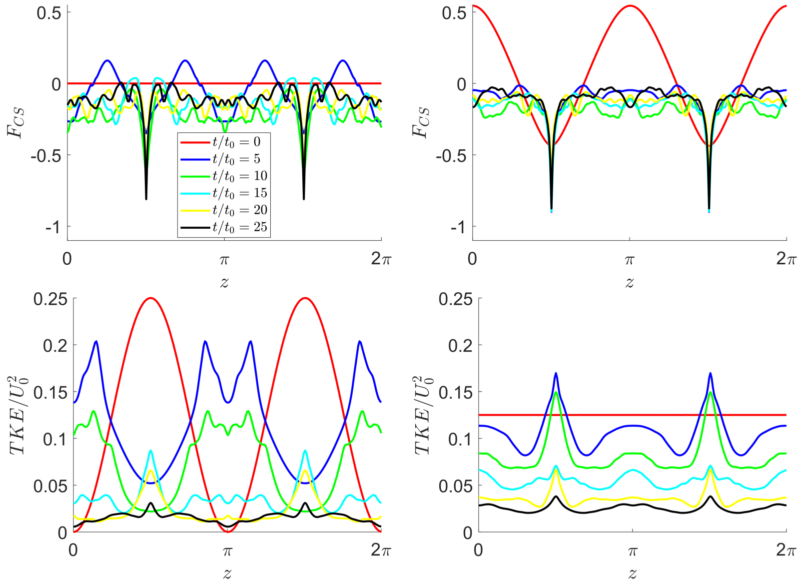

Figure 8. Coherent structure function (top) and TKE (bottom) averaged in the $x-y-$plane plotted over z/l_0 at different times for the *standard* TGV (left) and the *isotropic* TGV (right)

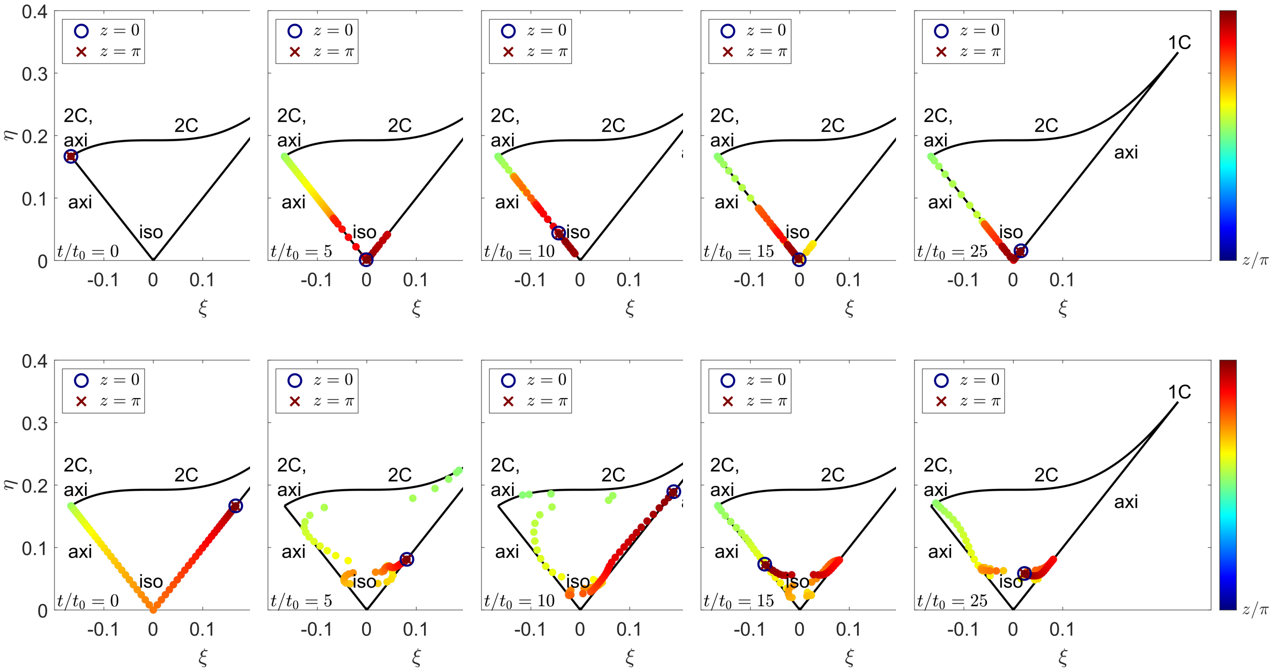

Figure 9. Lumley triangle for $x-y-$plane averaged Reynolds stresses as a function of z/l_0 at different times for the *standard* TGV (top) and the *isotropic* TGV (bottom)

proaches a state consistent with homogeneous isotropic turbulence. While small-scale quantities may exhibit increased isotropy, large-scale structures and spatial organization remain strongly influenced by the initial conditions and the periodic domain.

CONCLUSION

This study examined the isotropy and homogeneity of the *standard* and *isotropic* Taylor-Green vortex (TGV) using high-order numerical simulations. Both configurations were analyzed using classical turbulence statistics and homogeneity indices. The *standard* TGV exhibits persistent anisotropy and inhomogeneity even at late decay stages, with unequal integral length scales. The *isotropic* TGV, although globally isotropic by construction, does not satisfy the conditions of homogeneous isotropic turbulence. Both configurations display spatial inhomogeneities in the z direction, characterized by persistent peaks in the coherent structure function and turbulent kinetic energy at $z/l_0 = \pi/2, 3\pi/2$. These features originate from the symmetry of the initial conditions and are maintained by the triply periodic domain, indicating limited homogenization during decay. In summary, neither configuration achieves true homogeneous isotropic turbulence. This should be taken into account when using the TGV, particularly the *standard* case, as a benchmark for turbulence modeling or for isotropy-based assumptions.

REFERENCES

Bardos, C., Lopes Filho, M.C., Niu, D., Nussenzveig Lopes, H.J. & Titi, E.S. 2013 Stability of two-dimensional viscous incompressible flows under three-dimensional perturbations and inviscid symmetry breaking. *SIAM Journal on Mathematical Analysis* **45** (3), 1871–1885.

Brachet, M.E., Meiron, D.I., Orszag, S.A., Nickel, B.G., Morf, R.H. & Frisch, U. 1983 Small-scale structure of the Taylor-Green vortex. *Journal of Fluid Mechanics* **130**, 411–452.

Caban, L., Tyliszczak, A. & Geurts, B.J. 2026 Analysis of the impact of numerically induced high-order filters and regularization on LES modelling of an incompressible 3D Taylor-Green vortex flow undergoing laminar-turbulent transition. *Computers & Fluids* **312**, 107015.

Domaradzki, J.A., Liu, W. & Brachet, M.E. 1993 An analysis of subgridscale interactions in numerically simulated isotropic turbulence. *Physics of Fluids A: Fluid Dynamics* **5** (7), 1747–1759.

Engelmann, L., Hasslberger, J., Baik, SJ., Klein, M. & Kempf, A. 2023 Direct numerical simulation of an unsteady wall-bounded turbulent flow configuration for the assessment of large-eddy simulation models. *Scientific Reports* **13**, 11202.

Errante, M., Klein, M., Ferrero, A., Larocca, F., Scovazzi, G. & Germano, M. 2024 Mixed averaging procedures. *Flow, Turbulence and Combustion* **112**, 1001–1008.

Frisch, U. 1995 *Turbulence: The Legacy of A. N. Kolmogorov*. Cambridge: Cambridge University Press.

Germano, M. 1992 Turbulence: the filtering approach. *Journal of Fluid Mechanics* **238**, 325–336.

Hasslberger, J., Reissmann, M., Sandberg, R. D. & Klein, M. 2025 Exploiting semantic backpropagation to impose near-wall constraints in machine-learned symbolic subgrid-scale closures. *Physics of Fluids* **37** (3), 035203.

Hickel, S., Adams, N.A. & Domaradzki, J.A. 2006 An adaptive local deconvolution method for implicit LES. *Journal of Computational Physics* **213** (1), 413–436.

Hillewaert, K. 2011 Direct Numerical Simulation of the Taylor–Green Vortex at Re=1600. Test case: C3.5. Reference data from the 1st International Workshop on High-Order CFD Methods, available online at `https://cfd.ku.edu/hiocfd.html`.

Klein, M., Tyliszczak, A., Hasslberger, J. & Germano, M. 2026 Isotropy and homogeneity of the Taylor–Green vortex at late stages using different initial conditions. *Journal of Fluid Mechanics* **1032**, A36.

Kobayashi, H. 2005 The subgrid-scale models based on coherent structures for rotating homogeneous turbulence and turbulent channel flow. *Physics of Fluids* **17** (4), 045104.

Kolmogorov, A.N. 1941 The local structure of turbulence in incompressible viscous fluid for very large Reynolds numbers. *C.R. Acad. Sci. U.R.S.S.* **30**, 301.

Kulikov, Y.M. & Son, E.E. 2018 On the construction of turbulent transfer spectral models using 3D numerical simulation of Taylor-Green vortex decay. *High Temperature* **56** (6), 921–926.

Lumley, J.L. 1979 Computational modeling of turbulent flows. *Advances in applied mechanics* **18**, 123–176.

Nathen, P., Haussmann, M., Krause, M.J. & Adams, N.A. 2018 Adaptive filtering for the simulation of turbulent flows with lattice Boltzmann methods. *Computers & Fluids* **172**, 510–523.

Ono, A., Chitose, M., Suzuki, H. & Kouchi, T. 2024 Assessing OpenFOAM-based large-eddy simulation using decay characteristics of an isotropic Taylor-Green vortex. *Journal of Physics: Conference Series* **2694** (1), 012004.

Orszag, S.A. 1974 Numerical simulation of the Taylor-Green vortex. In *Computing Methods in Applied Sciences and Engineering Part 2* (ed. R. Glowinski & J. L. Lions), pp. 50–64. Berlin, Heidelberg: Springer Berlin Heidelberg.

Pope, S.B. 2000 *Turbulent flows*. Cambridge University Press.

Reissmann, M., Hasslberger, J., Sandberg, R.D. & Klein, M. 2021 Application of gene expression programming to a-posteriori les modeling of a Taylor Green vortex. *Journal of Computational Physics* **424**, 109859.

Taylor, G.I. & Green, A.E. 1937 Mechanism of the production of small eddies from large ones. *Proceedings of the Royal Society of London. Series A - Mathematical and Physical Sciences* **158** (895), 499–521.

Tyliszczak, A. 2014 A high-order compact difference algorithm for half-staggered grids for laminar and turbulent incompressible flows. *Journal of Computational Physics* **276**, 438–467.

Tyliszczak, A. 2016 High-order compact difference algorithm on half-staggered meshes for low Mach number flows. *Computers and Fluids* **127**, 131–145.